Radiocarbon, Vol 60, Nr 2, 2018, p 691–704 DOI:10.1017/RDC.2017.143

LARGE VARIABILITY OF DISSOLVED INORGANIC RADIOCARBON IN THE KUROSHIO EXTENSION OF THE NORTHWEST NORTH PACIFIC

Ling Ding[1] • Tiantian Ge[1] • Huiwang Gao[2] • Chunle Luo[1] • Yuejun Xue[3] • Ellen R M Druffel[4] • Xuchen Wang[1,3*]

[1]Key Laboratory of Marine Chemistry Theory and Technology, Ministry of Education, Ocean University of China, Qingdao 266100, China.
[2]Key Laboratory of Marine Environment and Ecology, Ministry of Education, Ocean University of China, Qingdao 266100, China.
[3]Ocean Science Isotope and Geochronology Center, Qingdao National Laboratory for Marine Science and Technology, Qingdao 266237, China.
[4]Department of Earth System Science, University of California, Irvine, CA 92697-3100, USA.

ABSTRACT. Radiocarbon (^{14}C) in dissolved inorganic carbon (DIC) was measured for water samples collected from six deep stations in the Kuroshio Extension (KE) region in the northwestern North Pacific in April–May 2015. Vertical profiles of $\Delta^{14}C$-DIC indicate that bomb-produced ^{14}C was present from the surface to ~1500 m water depth. Large variations in $\Delta^{14}C$-DIC values (300‰) were observed at 500 m water depth among the stations and the differences were likely controlled by transport and mixing dynamics of different water masses in the region. The major Pacific western boundary currents, such as Kuroshio and Oyashio and regional mesoscale eddies, could play important roles affecting the observed $\Delta^{14}C$-DIC variability. The depth profiles of both $\Delta^{14}C$-DIC and DIC concentrations can be predicted by the solution mixing model and can be used as conservative tracers of water mass movement and water parcel homogenization in the ocean.

KEYWORDS: dissolved inorganic carbon, Kuroshio Extension, North Pacific Intermediate Water, northwest North Pacific, radiocarbon.

INTRODUCTION

Dissolved inorganic carbon (DIC) is the largest exchangeable pool of carbon in the ocean and is biogeochemically important because it is directly linked to the organic carbon pool through photosynthesis and respiration. The variability of DIC in the ocean is controlled not only by anthropogenic CO_2 invasion (Winn et al. 1998; Tsunogai 2000) but also by changes in ocean circulation and biological activities (Tsurushima et al. 2002; Wakita et al. 2010; Gruber 2011). Radiocarbon (^{14}C) measurement of DIC has been a powerful tool to study carbon cycling (Broecker et al. 1995; Levin and Hesshaimer 2000), and circulation and transport of water masses in the ocean (Broecker et al. 1985; Key 1996; Druffel et al. 2008; Kumamoto et al. 2013). In the last few decades, bomb ^{14}C produced in the late 1950s and early 1960s entered the ocean through air–sea gas exchange and has provided an ideal tracer for short time scale (decades) water transport and circulation studies in the ocean (Stuiver and Östlund 1980; Stuiver et al. 1983; Druffel 1987; Broecker et al. 1995). During the Geochemical Ocean Section Study (GEOSECS) in the 1970s, the World Ocean Circulation Experiment (WOCE) in the 1990s and the ongoing Climate Variability and Predictability Program (CLIVAR), a large number of DIC samples were collected from the world oceans and $\Delta^{14}C$ measurements were reported (Östlund and Stuiver 1980; Key 1996; Stuiver et al. 1996; McNichol et al. 2000). These measurements have provided great insight into our understanding of the oceanic carbon cycle and ocean circulation processes, as linked to climate variability (examples are Stuiver et al. 1983; Broecker et al. 1995; Key et al. 1996; Druffel et al. 2008; Kumamoto et al. 2013; Sarnthein et al. 2013).

The northwest North Pacific (NP) is an important, highly dynamic region (Figure 1) where the Kuroshio Current (KC) and Oyashio Current (OC) mixes in the inter-frontal zone off the east coast of Japan, and the Kuroshio Extension (KE) flows eastward into the North Central Pacific (NCP) (Yasuda et al. 1996; Talley 1997; Qiu and Chen 2011). The NP Intermediate Water

*Corresponding author. Email: xuchenwang@ouc.edu.cn.

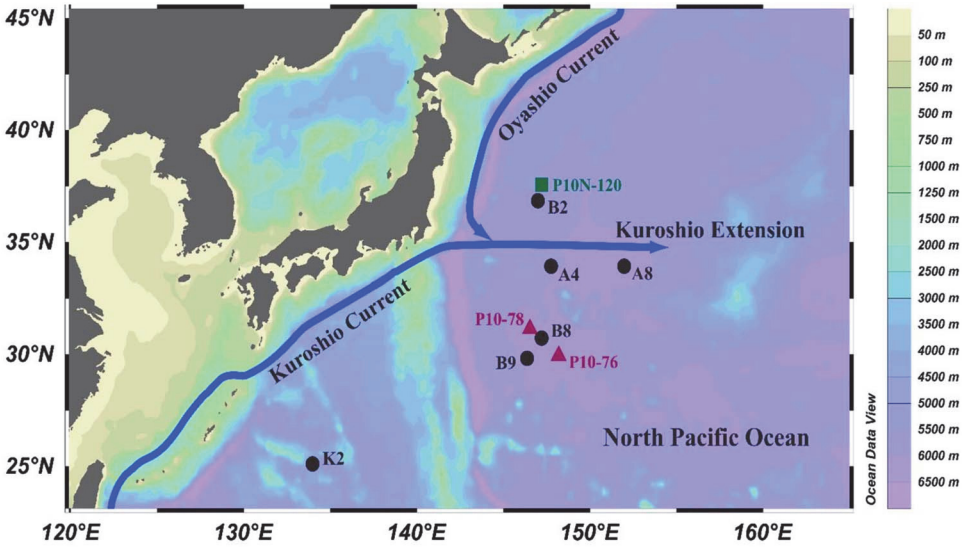

Figure 1 Map showing the study site and the six sampling stations (marked with black circles) in the northwestern North Pacific in April–May 2015. For comparison, we also plot three stations studied previously. Stations P10-76 and P10-78, which are close to our B8 and B9 stations, were from the WOCE P10 line collected in 1993 (Key et al. 1996), and station P10N-120, which is close to our B2 station, was collected in 2005 during a repeating cruise (MR05-02) to P10 line by Japanese scientists referred to as P10N line (Kumamoto et al. 2013).

(NPIW), which is formed in the mixed water region between the KE and Oyashio front (Talley 1993), plays an important role, not only for its impacts on the global ocean circulation and regional climate variability (Yasuda et al. 1996; Qiu and Chen 2011; Wu et al. 2012; Hu et al. 2015), but also as a major sink for anthropogenic carbon dioxide in the northwest NP (Tsunogai et al. 1993). In the last two decades, many studies were conducted using chemical tracers such as ^{14}C and chlorofluorocarbons (CFCs) to investigate the spatial and temporal variability of NPIW and its role influencing regional climate (Broecker et al. 1982; Tsunogai et al. 1995; Tokieda et al. 1996; Takatani et al. 2012; Kumamoto et al. 2013). In a recent study, Kumamoto et al. (2013) reviewed the decadal changes in bomb-produced ^{14}C measured in DIC in the NP from the 1990s to the 2000s. By comparing the differences in decadal changes of vertical profiles of $\Delta^{14}C$-DIC, they found that the inventory of bomb ^{14}C in the northwestern subtropical region decreased more significantly than that in the southern subtropical region due mostly to the ^{14}C decrease in the upper thermocline. The decadal variations in bomb ^{14}C in the NP indicate that the turnover time of thermocline circulation in the northwestern subtropical region is faster than that in the southern subtropical region as related to the transport of NPIW (Kumamoto et al. 2013). Using seven years (2002–2008) of surface DIC concentration data, Yasunaka et al. (2014) reported that the observed surface DIC seesaw variations in the NP was related to the Pacific Decadal Oscillation (PDO).

It has been 10 years since the collection of water samples for ^{14}C measurement in the northwestern NP reported by Kumamoto et al (2013). In this paper, we present $\Delta^{14}C$-DIC results of samples collected from six deep stations in the KE region in the northwestern NP in 2015. We observed large spatial variations in $\Delta^{14}C$-DIC values in the upper 1500 m among the stations. These variations in $\Delta^{14}C$-DIC profiles thus could provide useful information for our understanding of the water mass movement and mixing dynamics in the KE region.

METHODS

Oceanographic Setting

Our study sites in the western NP covered an area from 25° to 37°, and 134° to 152° (Figure 1). This is the region that is influenced largely by two major oceanic currents, the Kuroshio and Oyashio currents, which carry NPIW as part of the Pacific western boundary currents (Yasuda et al. 1996; Qiu and Chen 2011; Hu et al. 2015). The northeastward-flowing Kuroshio Current separates from the coast of Japan at about 34°, 140° and flows eastward as the Kuroshio Extension into the North Central Pacific (NCP) (Yasuda et al. 1996; Qiu and Chen 2011). The Oyashio is a southward-flowing current along the east coast of Japan carrying cold and fresh subarctic water. At about 37°, the Oyashio front meets the KE and forms the Kuroshio-Oyashio interfrontal zone, where the subarctic water mass mixes with the relatively warm and saline KE water, and flows eastward (Yasuda et al. 1996; Yasuda 2004; Hu et al. 2015). The newly formed NPIW is characterized by a salinity minimum zone in the density range of 26.6–27.4 due to the along isopycnal mixing between the Kuroshio and Oyashio waters, and consists of ~55% Kuroshio and 45% Oyashio waters (Talley et al. 1995; Talley 1997; Yasuda et al. 1996). The new NPIW is transported eastward by the KE as a low salinity tongue, with eventual mixing into the intermediate layers of the NP subtropical gyre (Yasuda et al. 1996; Qiu and Chen 2011). Long-term satellite data analyses have shown that the KE has undergone decadal oscillations between the elongated state and the contracted state, which affects both oceanic circulation and climate variations in the western NP (Qiu and Chen 2011; Hu et al. 2015). Recent studies have demonstrated that sub-mesoscale dynamics, such as eddies in the KE, undergo seasonal cycles and play an important role regulating the surface currents in the region (Ma et al. 2016; Rocha et al. 2016). Our study sites fall within the Kuroshio-Oyashio interfrontal zone of the KE (Figure 1).

Study Sites and Sample Collection

Water samples were collected at six stations on the *R/V* Dongfanghong-2 a cruise from March 31 to May 7 in 2015 (Table 1, Figure 1). The other three stations: P10-76 and P10-78 (red triangles) and P10N-120 (green square) are from previous studies (Key 1996; Kumamoto et al. 2013). The deepest bottom depth in the KE region is 6200 m, however we collected samples down to only 4000 m (due to an unexpected technical problem). Water samples were collected using 12-L Niskin bottles deployed on a rosette with CTD. For DIC water collection, we used the protocol described in McNichol and Jones (1991). Water was collected

Table 1 Description of the sampling site in the northwestern North Pacific

Station #	Location	Water depth (m)	Description
K2	25°06.094′N, 134°01.255′E	4100	East Kuroshio, subtropical gyre region
A4	34°00.018′N, 147°47.793′E	5800	Kuroshio-Oyashio interfront and KE
A8	34°02.350′N, 152°01.303′E	5500	Kuroshio-Oyashio interfront and KE
B2	37°00.237′N, 147°00.237′E	5580	North KE, east Oyashio, subpolar gyre
B8	30°58.048′N, 146°59.228′E	6000	South KE, recirculation zone
B9	29°51.711′N, 146°51.726′E	5500	Further south KE, recirculation zone

KE: Kuroshio Extension.

(after overflowing ~100 mL) in prebaked 100-mL glass bottles, with fine ground-glass stoppers, using precleaned silicone tubing connected directly to the Niskin bottle. After adding 50 µL saturated $HgCl_2$ solution, the bottles were capped tightly with grease-coated, ground-glass stoppers and secured with rubber bands to make a gas-tight seal to avoid any CO_2 exchange with atmosphere. All samples were kept in the dark at room temperature.

DIC Extraction and Concentration Analysis

After the cruise, DIC samples were processed in the laboratory within one month. DIC was extracted as gaseous CO_2 using our modified method (Ge et al. 2016) based on McNichol et al. (1994). Briefly, in a N_2 filled glove-bag, a 50 mL water sample was injected into a pre-evacuated 100-mL borosilicate glass bottle with ground-glass-joint stripping probes (precombusted at 550 for 4 hr). After injecting 1.0 mL high purity 85% H_3PO_4 using a glass syringe and stainless steel needle, the glass bottle with acidified water sample was placed in a hot water bath (70) for 30 min and shaken by hand several times. At pH ≤ 2, all forms of DIC (carbonate, bicarbonate, and CO_2) dissolved in water will become CO_2. It is calculated that at 70 under vacuum, the solubility of CO_2 in water is .0 × 10^{-5} µmol/L, so it is expected that all CO_2 dissolved in water has escaped into the probe headspace. The glass bottle was removed from the hot water bath and cooled for 5 min and connected to the vacuum line. All CO_2 generated was frozen into a liquid nitrogen trap. After the volume was measured manometrically, the CO_2 was flame-sealed inside 6-mm OD Pyrex tubes for ^{14}C and ^{13}C analyses. The extraction efficiency of DIC with the method was 6% (Ge et al. 2016).

Concentrations of DIC were measured using a Shimadzu TOC-L analyzer equipped with an ASI-V auto-sampler, using the total inorganic carbon (IC) mode. The concentration of DIC was calibrated using a 5-point calibration curve prepared from reagent grade sodium carbonate and sodium bicarbonate dissolved in DIC-free Milli-Q water as for the IC standard. The instrument blank and DIC values were checked against DIC reference materials (CRMs provided by Dr. A. Dickson at Scripps Institution of Oceanography, University of California San Diego). Total blanks associated with DIC measurements were less than 3.0 µM, which is 0.15% of seawater DIC concentrations, and the analytic precision of triplicate injections was %.

Isotopic Measurements

Both $\delta^{13}C$ and $\Delta^{14}C$ of DIC samples were analyzed at the National Ocean Sciences Accelerator Mass Spectrometry (NOSAMS) facility at Woods Hole Oceanographic Institution (WHOI). A small split of CO_2 was measured for $\delta^{13}C$ using a VG Isotope Ratio Mass Spectrometer (IRMS) and the remaining CO_2 was graphitized for $\Delta^{14}C$ analysis using AMS. Values of $\delta^{13}C$ are reported in ‰ relative to the VPDB standard and the ^{14}C measurements were reported as modern fraction (McNichol et al. 1994). The conventional radiocarbon ages (yr BP) were calculated using the Libby half-life as ascribed by Stuiver and Polach (1977). The total uncertainty of $\Delta^{14}C$-DIC and $\delta^{13}C$-DIC analyses are 6‰ and 0.1‰ or better, respectively, tested with a DIC standard (Ge et al. 2016).

RESULTS

The hydrographic data, DIC concentrations and isotopic results measured for 64 samples collected from the six stations are summarized in Table 2.

Table 2 Concentration and carbon isotopic ($\delta^{13}C$ and $\Delta^{14}C$) compositions of DIC measurements in the water samples collected from the western North Pacific.

Station	Water depth (m)	Temp. (℃)	Salinity (‰)	DIC (μmol/kg)	$\delta^{13}C$ (‰)	$\Delta^{14}C$ (‰)	Age (BP)
K2 (25□6.094′N, 134□1.255′E)							
	5	24.40	34.982	1848	0.2	45	Modern
	50	21.26	34.990	1839	0.3	50	Modern
	100	20.26	34.904	1867	0.2	49	Modern
	200	18.37	34.785	1892	0.1	60	Modern
	300	16.51	34.670	1918	0.1	56	Modern
	500	10.86	34.297	1867	–1.1	38	Modern
	650	6.81	34.151	2056	–0.6	–64	470
	1000	3.90	34.372	2110	–0.5	–180	1530
A4 (34□0.018′N, 147□7.793′E)							
	5	17.50	34.759	1822	–0.1	51	Modern
	50	17.18	34.762	1806	0.1	45	Modern
	100	16.98	34.765	1824	–0.1	49	Modern
	200	16.84	34.752	1836	0.1	45	Modern
	500	14.22	34.512	2088	–0.2	–233	2070
	750	7.80	34.114	2087	–0.6	–231	2050
	1000	4.75	34.147	2063	–0.1	–229	2020
	2000	2.21	34.554	1975	–0.3	–226	2015
	3000	1.64	34.655	2120	–0.4	–233	2070
	4000	1.51	34.681	2119	–0.4	–220	1930
A8 (34□2.359′N, 152□1.303′E)							
	5	17.70	34.791	1798	0.3	48	Modern
	60	17.14	34.784	1834	0.2	50	Modern
	100	16.93	34.761	1855	–0.1	41	Modern
	250	16.76	34.744	1850	–0.1	47	Modern
	500	12.55	34.400	1887	–0.1	22	Modern
	650	8.88	34.089	1876	0.1	30	Modern
	1000	4.27	34.199	2056	–0.5	–137	1120
	1500	2.76	34.452	2130	–0.6	–205	1780
	2000	2.15	34.562	2112	–0.2	–230	2040
	3000	1.62	34.656	2141	–0.4	–231	2050
	3500	1.53	34.672	2138	–0.1	–222	1960
B2 (37□0.237′N,147□0.237′E)							
	5	14.72	34.490	1850	0.5	31	Modern
	50	13.58	34.429	1875	0.1	20	Modern
	100	11.24	34.315	1920	–0.3	1	Modern
	200	6.50	33.662	1926	–0.1	–8	Modern
	350	5.52	33.759	2063	–0.7	–125	1010
	500	4.31	34.039	2067	–0.6	–106	840
	750	3.67	34.287	2115	–0.9	–166	1400
	1000	3.03	34.405	2102	–0.3	–234	2080
	1500	2.32	34.527	2125	–0.1	–226	1990
	2000	1.92	34.601	2108	–0.4	–219	1920
	3000	1.55	34.666	2050	–0.3	–220	1930
	4000	1.47	34.685	2080	–0.1	–228	2020

Table 2: (*Continued*)

Station	Water depth (m)	Temp. (℃)	Salinity (‰)	DIC (μmol/kg)	$\delta^{13}C$ (‰)	$\Delta^{14}C$ (‰)	Age (BP)
B8 (30°58.048′N,146°59.228′E)							
	5	19.42	34.877	1833	–0.2	49	Modern
	50	18.73	34.884	1829	0.1	52	Modern
	100	18.44	34.863	1854	0.1	50	Modern
	200	17.65	34.772	1854	–1.5	3	Modern
	500	11.79	34.330	1901	–0.3	–99	775
	800	4.92	34.076	1893	–0.6	–105	830
	1000	3.90	34.260	2073	–0.8	–157	1310
	1500	2.56	34.490	1973	–0.1	–197	1700
	2000	1.97	34.595	2008	–0.1	–213	1860
	2500	1.72	34.640	1997	0.2	–219	1930
	3000	1.57	34.662	2008	–0.2	–212	1850
	3500	1.51	34.675	2006	–0.1	–212	1850
B9 (29°51.711′N,146°51.726′E)							
	5	20.69	34.895	1866	–0.1	42	Modern
	30	19.05	34.900	1858	–0.2	32	Modern
	100	17.77	34.814	1870	–0.6	27	Modern
	150	17.55	34.796	1865	–0.5	26	Modern
	200	17.52	34.789	1858	–1.9	18	Modern
	300	17.11	34.749	1848	–0.3	31	Modern
	500	13.22	34.440	1863	–0.4	15	Modern
	700	6.78	34.050	1961	–0.5	–59	425
	1000	3.15	34.400	2029	–0.1	–159	1330
	1500	2.54	34.511	2014	0.1	–220	1930
	2000	1.98	34.602	2052	–0.6	–222	1960

Hydrographic Profiles

Figure 2 shows the temperature, salinity, and density profiles for the six stations. Temperature (T) decreased rapidly from the surface to about 1500 m depth and then remained constant for all stations (Figure 2a). The largest differences in the T profiles appear in the upper 600 m depth, where Sta K2 had the highest T (24.40℃) and Sta B2 had the lowest T (14.72℃) in the surface layer (5 m). Water temperature profiles for stations A4, A8, B8, and B9 showed less variation and decreased in parallel from the surface (17.5–20.7℃) to about 2.5℃ at 1500 m and then remained the same below 1500 m (Figure 2a). Salinity decreased from the surface initially and then increased with depth to about 2500 m. Below 2500 m, the salinity for all stations were the same and remained relatively constant. Like T, the largest variations in S profiles are also seen in the upper 500 m depth. Sta B2 had the lowest salinity (34.490) in the surface and decreased to 33.662 by 250 m, then increased to similar values as the other five stations at 2500 m. The S profiles for stations K2, A4, A8, B8, and B9 showed less variations in the surface water (5 m) (34.877–34.982) and Sta K2 had the highest S value (34.982) among all stations in the surface. The potential density profiles also clearly show the distinct water masses in the upper 1000 m depth (Figure 2c) with large differences among the stations. Sta B2 had the highest potential density in the upper 1000 m depth, and Sta K2 had the lowest water density values in the upper 200 m, respectively.

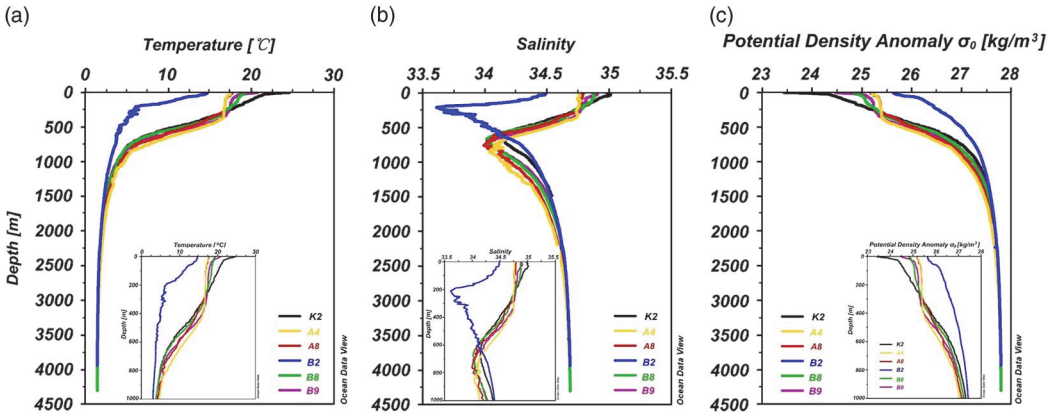

Figure 2 Temperature, salinity and potential density profiles for the six stations in the northwestern North Pacific sampled in April–May 2015. The insert figure shows the profile in the upper 1000 m depth.

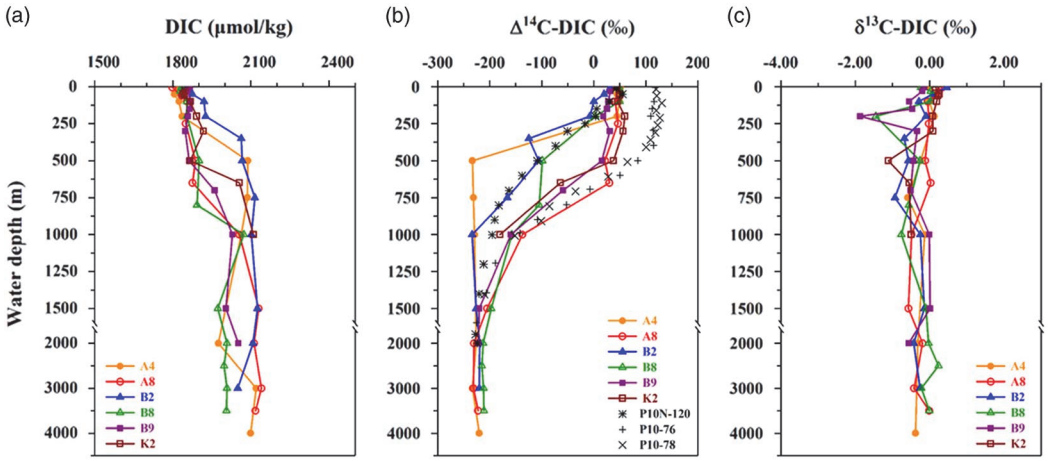

Figure 3 Depth profiles of DIC, Δ^{14}C-DIC and δ^{13}C-DIC measured for the six stations in the northwestern North Pacific sampled in April–May 2015. In Figure 3b, the depth profiles of Δ^{14}C-DIC for stations P10-76, P10-78, and P10N-120 are plotted for comparison (see Discussion). Note: the depth scale below 1500 m has been reduced.

DIC and Isotopic Distributions

Profiles of DIC concentration and their isotopic values for the six stations are shown in Figure 3. For the Δ^{14}C-DIC profiles (Figure 3b), we also plot three stations studied earlier for comparison (Figure 1). Stations P10-76 and P10-78 that are close to our B8 and B9 stations were from the WOCE P10 line collected in 1993 (data provided by Dr. Robert Key at Princeton University). Station P10N-120 that is close to our B2 station was collected in 2005 during a repeat cruise (MR05-02) to the P10 line by Japanese scientists referred to as the P10N line (Kumamoto et al. 2013). These stations in the same region were sampled ~10 years apart, so they provide data comparison for the last 22 years (1993–2015).

Concentrations of DIC ranged from 1798 to 2141 μmol/kg (Figure 3a, Table 2). In general, concentrations of DIC showed similar values in the surface water (5 m) and increased with depth even though the trend exhibited some variations among the stations (Figure 3a).

Concentrations of DIC showed less variation in the upper 200 m and all increased at depths below 200 m. The most variability in DIC concentration at all stations was observed between 400–1000 m depths. For the four deep stations (A4, A8, B2, and B8), concentrations of DIC for A8 and B8 remained relatively constant from 1500–3500 m; decreased in the middle depth (2000 m) and then increased and remained constant at 3000–4000 m for station A4; and slightly decreased from 2000–4000 m depth at station B2 (Figure 3a). Station A8 in the middle of the KE had the highest DIC concentrations (2130–2141 μmol/kg) from 1500–3500 m.

Values of Δ^{14}C-DIC in the surface water (5–50 m) ranged from 20‰ to 52‰ for the six stations and all decreased with depth to –200‰ to –220‰ at about 1500 m, then remained relatively constant in the deeper waters (Figure 3b). As for T and S profiles, large variations in Δ^{14}C-DIC were seen in the upper 1000 m among the stations. Values of Δ^{14}C-DIC from Sta A4 decreased to the lowest values (–233‰) by 500 m, a 278‰ drop in Δ^{14}C values in just 300 m of the water column. Below 500 m, the Δ^{14}C-DIC values for Sta A4 remained constant down to 4000 m. Values of Δ^{14}C-DIC at Sta B2 also showed a rapid decrease from 32‰ in the surface to –234‰ at 1000 m depth, then remained similar to those at Sta A4 by 4000 m depth (Figure 3b). Δ^{14}C-DIC for Sta B8 decreased rapidly, first from the surface value (49‰) to –99‰ at 500 m, and then to –197‰ at 1500 m. The Δ^{14}C-DIC profiles for the stations K2, A8, and B9 exhibited a similar trend, showing relatively constant values in the upper 500–600 m and then decreased to 1500 m (1000 m for K2). At 500-m depth, there were much lower Δ^{14}C values at A4 compared with those at A8, B9, and K2 (Figure 3b). The differences of the Δ^{14}C-DIC profiles between our stations and those from the three earlier stations are presented in the Discussion section.

The δ^{13}C-DIC values from the six stations ranged from 0.46‰ to –1.87‰, and the highest variation appeared in the depths from 100–500 m (Figure 3c). Values of δ^{13}C-DIC showed a low peak for stations B8 and B9 at 200 m depth, and K2 at ~500 m depth. Below 500 m depth, the δ^{13}C-DIC values were generally constant for all stations.

DISCUSSION

Variability of ^{14}C-DIC in the Kuroshio Extension

The KE is a highly dynamic region where the Kuroshio and Oyashio Currents meet and influence the hydrology and chemical properties of the resulting water mass (Tsunogai et al. 1995; Tsurushima et al. 2002). The DIC concentration and isotopic profiles for the six stations (Figure 3) indicate the influence of different water masses in the region, especially in the upper 1000 m of the water column. In Figure 4, we plot T versus salinity with DIC concentrations and Δ^{14}C-DIC values (as the colors of the points) associated with the potential density anomaly. It can be clearly seen that the distributions of both DIC concentrations and Δ^{14}C-DIC were associated with different density water masses in the region (groups of circled points). High DIC concentrations and low Δ^{14}C-DIC values were present in denser waters (σ_0 27.0), while lower DIC concentrations and high Δ^{14}C-DIC values were present in lower density water masses (σ_0 25.5) (Figure 4). The denser water masses likely originated from the subarctic gyre, which circulates with the NPIW and has low T and S values. Based on the field observations, Yasuda (2004) reported that NPIW circulation in the subarctic gyre is related to diapycnal-meridional overturning, generated around the Okhotsk Sea due to tidal-induced diapycnal mixing and dense shelf water formation accompanied by sea-ice formation; and transport through the south-flowing Oyashio along the western boundary from the subarctic to KE region. The lower density water masses with high T and S, however, were transported by the northeast-flowing Kuroshio Current and mixed with Oyashio water in the KE region (Figure 2).

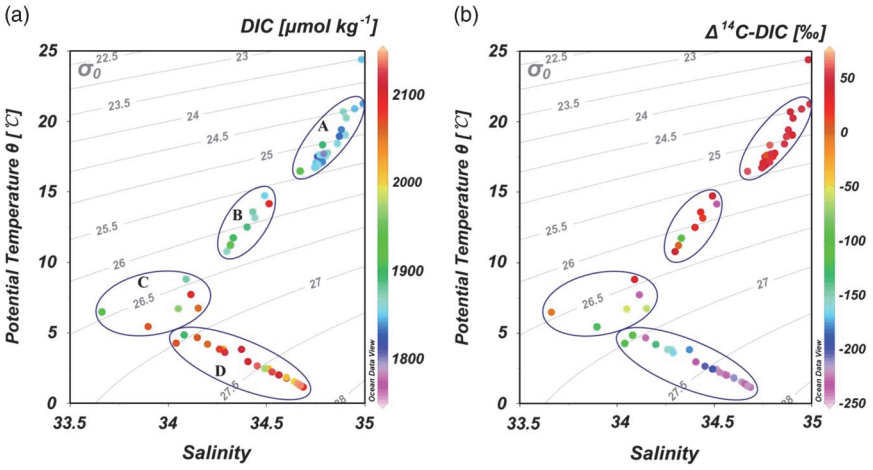

Figure 4 Plot T versus salinity with (a) DIC concentration and (b) Δ^{14}C-DIC values (indicated as colors) for all samples measured for the six stations in the northwestern North Pacific. Lines are constant potential density. The circular areas represent different water masses as (A) lighter water mass in the upper 300 m depth with lower DIC and higher Δ^{14}C-DIC; (B) mixed upper water in 300–500 m depth; (C) mixed intermediate water in 500–800 m depth; and (D) denser NP deep water in [illegible]000 m depth. The one outlier at the right-top is the surface water of Station K2. (Colors refer to online version.)

Examination of the Δ^{14}C-DIC profiles reveals that Sta K2, which is on the path of the north-flowing Kuroshio Current, is a region that transports water with relatively higher Δ^{14}C-DIC values in the upper 500 m (38–60‰). These Δ^{14}C-DIC values shows that bomb ^{14}C was well mixed down to 500 m depth in the Kuroshio Current (Figure 3b). For stations A8 and B9 in the KE region, the Δ^{14}C-DIC profiles also showed similar high bomb ^{14}C signals that were mixed down to ~500 m depth, likely influenced by the Kuroshio water mass. In comparison, for stations A4 and B8, the well-mixed high bomb ^{14}C signal was observed in the upper 150–250 m only and the Δ^{14}C-DIC values decreased rapidly with depth (Figure 3b). As discussed above, the Δ^{14}C-DIC profiles for stations B2, A4 and B8 appear to be influenced by the Oyashio Current, which carries subarctic NPIW southward and mixes with the Kuroshio water in the region around 35–37[illegible]N and 143[illegible]east (Yasuda et al. 1996; Qiu and Chen 2011). In its path, this subarctic water mass influences the T and S profiles of Sta B2 in the upper 600 m depth as being well demonstrated in Figure 2. And this subarctic water mass also carries higher DIC concentrations affecting stations B2 and A4 in the upper 700 m depth as well (Figure 3a).

To further demonstrate the influence of different water masses on the chemical properties in KE region, Figure 5 compares the cross sectional distributions for salinity, DIC concentration and Δ^{14}C-DIC for the four stations B2, A4, B8, and B9 as a line transect across the KE from 37[illegible]′ N to 29[illegible]′N. The regional influences of the two water masses carried by the Kuroshio and Oyashio currents can be seen more clearly in Figure 5. It appears likely that the subarctic water with low salinity, high DIC concentrations and low Δ^{14}C-DIC values carried by the Oyashio Current intruded southward to about 34[illegible]N in the upper 500 m at Sta A4 and mixed with the Kuroshio water to form the KE water mass. However, we are not able to determine if this southward intrusion of the Oyashio water reflects a seasonal change or a decadal oscillation of the NPIW.

It is possible that the large Δ^{14}C-DIC variability we observed between stations A4, B2 and others could be largely influenced by local water circulation, vertical mixing processes and/or

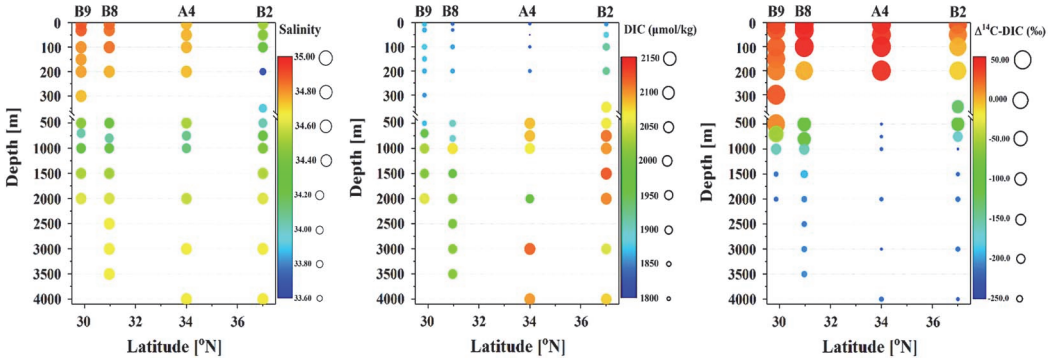

Figure 5 Comparison of cross section distributions of salinity, DIC concentration and Δ^{14}C-DIC values for stations B9, B8, A4, and B2 in the northwestern North Pacific.

mesoscale eddies in the KE region. Physical oceanographic studies have shown that the formation of the KE along the boundary between the NP subtropical and subarctic gyres is hydrodynamically unstable, thus allowing vigorous ocean eddies to form in the KE region (Qiu and Chen 2011; Waterman et al. 2011; Ma et al. 2016). In their recent study, Rocha et al. (2016) reported that the seasonal change of upper ocean stratification in the KE also modulates submesoscale (10–100 km) inertia-gravity waves and turbulence. These inertia-gravity waves and turbulence could affect the chemical profiles in the region. Qiu and Chen (2011) also reported that the KE is an unstable current that can transport northern Oyashio-origin water southward through mesoscale eddies, causing the fresher Oyashio water to be "diffused" southward across the KE. The significant, low Δ^{14}C-DIC values we observed at stations B2 and A4 in the upper 200–1000 m depth could reflect this transport south via mesoscale eddies. A recent high-resolution coupled atmosphere-ocean model has revealed that local ocean mesoscale eddies and atmospheric feedback is fundamental to the dynamics governing the KE variability (Ma et al. 2016). If this is the case, we could expect that the southward intrusion of the Oyashio Current that carries fresh, cold, nutrient-rich, high DIC subarctic NPIW could have a significant influence on the chemical and biological processes in the KE region. Nutrient-rich NPIW could enhance primary production in the region, and thus increase the net flux of atmospheric CO_2 into the surface ocean. The cold, subarctic water mixing with warm Kuroshio water could also reduce the heat transfer to the atmosphere, and thus affect the regional climate (Wu et al. 2012; Hu et al. 2015; Ma et al. 2016).

The depth profiles of δ^{13}C-DIC for the stations show large variations, mainly in the upper 500 m depth (Figure 3c). The relatively higher δ^{13}C-DIC values in the surface waters (0–50 m) reflect the influence of photosynthesis, which preferentially fix light ^{12}C into OC and thus leaves ^{13}C enriched DIC in the surface waters. On the other hand, sinking and remineralization of OC below the euphotic zone releases light CO_2, and may have caused the observed decrease of δ^{13}C-DIC values at 200–500 m depths at stations B9 and B8, respectively (Figure 3c). During our sampling in May–June 2015, we measured very low dissolved nitrogen (DN) concentrations ( μM in the upper 100 m; Ding et al. 2017) in the surface waters for the stations, suggesting the primary production was active in the region. This supports our DIC and Δ^{14}C-DIC profiles discussed above.

Comparison with Earlier  C-DIC Results

During the WOCE Program in the early 1990s, thousands of DIC samples were collected from the world oceans and their Δ^{14}C values reported (Key 1996; Stuiver et al. 1996; McNichol et al.

2000). Δ^{14}C-DIC measurements have provided considerable insight to the understanding of the oceanic carbon cycle and ocean circulation processes, as linked to climate variability. Here, we compare our Δ^{14}C-DIC results with those from three earlier stations in the KE region. As shown in Figure 3b, Stations P10–76 and P10–78 sampled in 1993 had much higher Δ^{14}C-DIC values (~130‰) in the surface and decreased rapidly down to 1500 m depth. Below 700–800 m depth, the Δ^{14}C-DIC profiles of P10–76 and P10–78 had similar values and decreased in parallel as our B8, B9, and A8 stations, suggesting that the same water mass was carried by the KE in the last 20 years. The higher Δ^{14}C-DIC values in the upper 700 m depth of stations P10–76 and P10–78 reflect the higher bomb–produced ^{14}C present in the surface down to 600 m depth in 1993. The different values of Δ^{14}C-DIC between the two P10 stations and B8 and B9 (80–90‰) in the surface was likely due to the decrease of the bomb Δ^{14}C signal in the atmosphere in the last 20 years that has mixed into the upper ocean through air–sea exchange. As reported by Hua et al (2013), the global average Δ^{14}C value in atmospheric CO_2 has decreased from ~150‰ in 1990 to ~50‰ in 2010, a 5‰ drop annually over the past 20 years. This has lowered the Δ^{14}C-DIC signature of the upper ocean, thus explaining the observed Δ^{14}C-DIC differences in the surface between the two P10 stations and our sites (Figure 3b). However, the large difference of Δ^{14}C-DIC (~150‰) between the two P10 stations and B8 in the depths of 200–500 m cannot be similarly explained. As can be seen, the Δ^{14}C-DIC profile of Sta B8 in the upper 500 m was the same as the Sta P10N-120 sampled in 2005. As discussed above, we expect that the Δ^{14}C-DIC profile in the upper 800 m depth at stations B2 and A4 were all influenced by the subarctic NPIW carried by the southward-flowing Oyashio Current during our sampling. The relatively lower Δ^{14}C-DIC values measured in the 250–500-m depth at Sta B8, however, could be affected by the seasonal or annual variations of the local circulation, vertical mixing and mesoscale eddies (Qiu and Chen 2011; Waterman et al. 2011; Ma et al. 2016) which upwelled some deep water with lower Δ^{14}C-DIC to the upper depth at Sta B8. More seasonal studies are needed to better answer these questions.

Application of Keeling Plot on DIC Mixing in KE

Keeling plot analysis has been performed on DIC depth profiles to discern consistency with solution based two-component mixing model (Beaupré and Aluwihare 2010). As plotted in Figure 6, there is a good correlation between Δ^{14}C-DIC and $[DIC]^{-1}$ (r^2 ≥0.84, p ≤0.001) in the KE, suggesting that both parameters were mainly controlled by the hydrodynamic mixing processes in the KE region. When separating the water samples into three depths, it can been seen that some deep water with low Δ^{14}C-DIC values were mixed into the upper water column (0–500 m). The slope (4.0×10^6) and intercept (–2026) values of the Keeling plot for the six stations in the KE are consistent with the values obtained in the South Ocean (5.64×10^6, –2670), eastern NP (4.29×10^6, –2040), and central NP (5.28×10^6, –2470) as reported by Beaupré and Aluwihare (2010).

When they examined large data sets of concentrations of DIC versus Δ^{14}C-DIC, Sarnthein et al. (2013) obtained regression slopes of –0.79 and –1.49 for the South Pacific and North Pacific, respectively. Our value of –0.85 (plot not shown) is also comparable to their values. These similarities indicate that the distribution of Δ^{14}C-DIC in the open ocean could be predicted by the solution mixing model and DIC can be used as a conservative tracer for water mass movement and water parcel homogenization (Beaupré and Aluwihare 2010). If we take an average Δ^{14}C-DIC value of 50‰ for the Kuroshio water in the upper 500 m depth (Sta K2) and –220‰ for the NPIW of Oyashio (Figure 6), we calculated based on the mass balance that 55–58% Oyashio water and 42–45% of Kuroshio water could be mixed at the depth of 500 m to result in the observed Δ^{14}C-DIC values (Figure 3b) at stations B2 and B8; 100% Oyashio water at Sta A4 and 96–100%

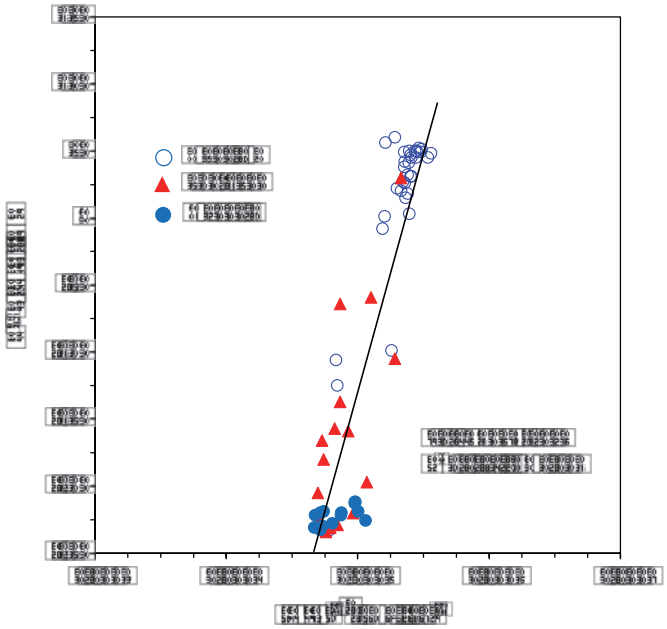

Figure 6 Keeling plot of Δ^{14}C-DIC versus concentration of [DIC] $^{-1}$ measured for the six deep stations in the Kuroshio Extension region in the northwest North Pacific. The line is a linear regression fit to all data points.

Kuroshio water at stations A8 and B9, respectively. These mixing ratios are clearly restricted to a surface water scenario where it is affected by the present state of the bomb signals. The more natural mixing dynamics of Δ^{14}C-DIC of water samples collected in 2000 m depth in the global oceans have been recently examined and referred to Sarnthein et al. (2013).

SUMMARY

The large variability of Δ^{14}C-DIC values that we observed in the KE in the northwestern NP revealed the complicated mixing dynamics of the different water masses that influence the chemical and isotopic distributions in the region. The results suggest that the low Δ^{14}C-DIC and high DIC profiles at stations A4 and B2 were largely affected by the Oyashio Current front which carries the cold and fresh subarctic intermediate water into the KE. In contrast, the relatively higher Δ^{14}C-DIC and low DIC profiles at stations A8, B9, and K2 were likely influenced by the northeast-flowing Kuroshio Current, which carries warm and high salinity water. The Δ^{14}C-DIC and DIC values can be used as relatively conservative tracers of water mass movement and mixing in the ocean. The large variability in the observed Δ^{14}C-DIC profiles could have also been caused by mesoscale eddies in the KE region. In any case, the intrusion of nutrient-rich subarctic water with low Δ^{14}C-DIC values could have an important influence not only on the regional production and ecosystem, but also on carbon cycling in the northwestern NP. Further studies are required to determine the actual temporal variability of this system.

ACKNOWLEDGMENTS

We thank Drs. Lixin Wu and Xiaopei Lin for providing the cruise opportunity and the crews of the *R/V* Dongfanghong-2 and Dr. Lei Li for the help during sample collection.

We thank Dr. Robert Key at Princeton University and Dr. Yuichiro Kumamoto at the Research Institute for Global Change, Japan Agency for Marine–Earth Science and Technology (JAMSTEC) for kindly providing the data for comparison. We also thank Dr. Ann McNichol and the staff and colleagues at the WHOI National Ocean Science Accelerator Mass Spectrometry (NOSAMS) facility for measurements of $\delta^{13}C$ and $\Delta^{14}C$ of the samples. We appreciate the thorough review and comments from Associate Editor P. Grootes and two reviewers. Financial support for this work was provided by China's National Natural Science Foundation (Grants: 91428101, 41476057) and the Fundamental Research Funds for the Central Universities (Grant: 201762009).

REFERENCES

Beaupré SR, Aluwihare L. 2010. Constraining the 2-component model of marine dissolved organic radiocarbon. *Deep-Sea Research II* 57(16): 1494–503.

Broecker WS, Peng TH, Ostlund GH, Stuiver M. 1985. The distribution of bomb radiocarbon in the ocean. *Journal of Geophysical Research* 90(C4):6953–70.

Broecker WS, Spencer DW, Craig H. 1982. GEOSECS Pacific Expedition, Volume 3. *Hydrographic Data 1973–1974*. Washington, DC: U.S. Government Printing Office. p 137.

Broecker WS, Sutherland S, Smethie W, Peng TH, Ostlund G. 1995. Oceanic radiocarbon: separation of the natural and bomb components. *Global Biogeochemical Cycles* 9(2):263–88.

Ding L, Ge TT, Gao HW, Zhang J, Wang XC. 2017. Dissolved organic carbon and total nitrogen in the East China Sea and the Kuroshio Extension of the northwest North Pacific. *Marine Chemistry* (in review).

Druffel ERM. 1987. Bomb radiocarbon in the Pacific: annual and seasonal timescale variations. *Journal of Marine Research* 45(3):667–98.

Druffel ERM, Bauer JE, Griffin S, Beaupré SR, Hwang J. 2008. Dissolved inorganic radiocarbon in the North Pacific Ocean and Sargasso Sea. *Deep-Sea. Research I* 55(4):451–9.

Ge TT, Wang XC, Zhang J, Luo CL, Xue YJ. 2016. Dissolved inorganic radiocarbon in the northwest Pacific continental margin. *Radiocarbon* 58(3): 517–29.

Gruber N. 2011. Warming up, turning sour, losing breath: ocean biogeochemistry under global change. *Philosophical Transactions of the Royal Society A* 369(1943):1980–96.

Hua Q, Barbetti B, Rakowski AZ. 2013. Atmospheric radiocarbon for the period 1950–2010. *Radiocarbon* 55(4):2059–72.

Hu DX, Wu LX, Cai WJ, Gupta AS, Ganachaud A, Qiu B, Gordon AL, Lin X, Chen Z, Hu S, Wang G, Wang Q, Sprintall J, Qu T, Kashino Y, Wang F, Kessler WS. 2015. Pacific western boundary currents and their roles in climate. *Nature* 522 (7556):299–308.

Key RM. 1996. WOCE Pacific Ocean radiocarbon program. *Radiocarbon* 38(3):415–23.

Key RM, Quay PD, Jones GA, McNichol AP, Reden KF, Schneider RJ. 1996. WOCE AMS radiocarbon I: Pacific Ocean Results (P6, P16 and P17). *Radiocarbon* 38(3):425–518.

Kumamoto Y, Murata A, Kawano T, Watanabe S, Fukasawa M. 2013. Decadal changes in bomb–produced radiocarbon in the Pacific Ocean from the 1990s to 2000s. *Radiocarbon* 55(2–3):1641–50.

Levin I, Hesshaimer V. 2000. Radiocarbon - A unique tracer of global carbon cycle dynamics. *Radiocarbon* 42(1):69–80.

Ma XH, Zhao J, Chang P, Liu X, Montuoro R, Small RJ, bryan FO, Greatbatch RJ, Brandt P, Wu D, Lin X, Wu L. 2016. Western boundary currents regulated by interaction between ocean eddies and the atmosphere. *Nature* 535(7613):533–7.

McNichol AP, Jones GA. 1991. Measuring ^{14}C in seawater $\sum CO_2$ by accelerator mass spectrometry, WHP operations and methods. In: Joyce T, Corry C, Stalcup M, editors. *WOCE Operations Manual. Part 3.1.2, Requirements for WHP Data Reporting*. Woods Hole, Massachusetts: WHPO Publication 90–1. p 71.

McNichol AP, Jones GA, Hutton DL, Gagnon AR. 1994. The rapid preparation of seawater $\sum CO_2$ for radiocarbon analysis at the national ocean sciences AMS facility. *Radiocarbon* 36(2): 237–46.

McNichol AP, Schneider RJ, von Reden KF, Gagnon AR., Elder KL, NOSAMS, Key RM, Quay PD. 2000. Ten years after–The WOCE AMS Radiocarbon Program. *Instruments and Methods in Physics. Research B* 172(1–4):479–84.

Qiu B, Chen S. 2011. Effect of decadal Kuroshio Extension jet and eddy variability on the modification of North Pacific Intermediate Water. *Journal of Physical Oceanography* 41(3):503–15.

Östlund HG, Stuiver M. 1980. GEOSECS Pacific radiocarbon. *Radiocarbon* 22(1):25–53.

Rocha CB, Gille ST, Chereskin TK, Menemenlis D. 2016. Seasonality of submesoscale dynamics in the Kuroshio Extension. *Geophysical Research Letters* 43(21):11, 304–11.

Sarnthein M, Schneider B, Grootes PM. 2013. Peak glacial ^{14}C ventilation ages suggest major drawdown of carbon into the abyssal ocean. *Climate of the Past* 9(6):2595–614.

Stuiver M, Polach HA. 1977. Discussion: reporting of ^{14}C data. *Radiocarbon* 19(3):355–63.

Stuiver M, Quay PD, Östlund HG. 1983. Abyssal water ^{14}C distribution and the age of the world oceans. *Science* 219(4586):849–51.

Stuiver M, Östlund HG. 1980. GEOSECS Atlantic radiocarbon. *Radiocarbon* 22(1):1–24.

Stuiver M, Östlund G, Key RM, Reimer PJ. 1996. Large volume WOCE radiocarbon sampling in the Pacific Ocean. *Radiocarbon* 38(3):519–61.

Takatani T, Sasano D, Nakano T, Midorikawa T, Ishii M. 2012. Decrease of dissolved oxygen after the mid-1980s in the western North Pacific subtropical gyre along the 137 repeat section. *Global Biogeochemical Cycle* 26(2):GB2013.

Talley LD. 1993. Distribution and formation of North Pacific Intermediate Water. *Journal of Physical Oceanography* 23:517–37.

Talley LD, Nagata Y, Fujimura M, Iwao T, Kono T, Inagake D, Hirai M, Okuda K. 1995. North Pacific Intermediate Water in the Kuroshio/Oyashio mixed water region. *Journal of Physical Oceanography* 25(4):475–501.

Talley LD. 1997. North Pacific Intermediate Water transports in the mixed water region. *Journal of Physical Oceanography* 27(8):1795–803.

Tokieda T, Watanabe S, Tsunogai S. 1996. Chlorofluorocarbons in the western North Pacific in 1993 and formation of North Pacific Intermediate Water. *Journal of Oceanography* 52(4):475–90.

Tsunogai S. 2000. North Pacific water's large potential sink capacity for absorbing anthropogenic CO_2 and the processes recovering it. In: Handa N, Tanoue E, Hama T, editors. *Dynamics and Characterization of Marine Organic Matter*. Tokyo: Terrapub. p 533–60.

Tsunogai S, Ono T, Watanabe S. 1993. Increase in total carbonate in the western North Pacific water and a hypothesis on the missing sink of anthropogenic carbon. *Journal of Oceanography* 49(3):305–15.

Tsunogai S, Watanbe S, Honda M, Aramaki T. 1995. North Pacific Intermediate Water studied chiefly with radiocarbon. *Journal of Oceanography* 51(5):519–36.

Tsurushima N, Nojiri Y, Imai K, Watanabe S. 2002. Seasonal variations of carbon dioxide system and nutrients in the surface mixed layer at station KNOT (44 N, 155 E) in the subarctic western North Pacific. *Deep-Sea Research II* 49(24–25):5377–94.

Wakita M, Watanabe S, Murata A, Tsurushima N, Handa M. 2010. Decadal change of dissolved inorganic carbon in the subarctic western North Pacific Ocean. *Tellus B* 62(5):608–20.

Waterman S, Hogg NG, Jayne SR. 2011. Eddy-mean flow interaction in the Kuroshio Extension region. *Journal of Physical Oceanography* 41(6):1182–208.

Winn CD, Li YH, Mackenzie FT, Karl DM. 1998. Rising surface ocean dissolved inorganic carbon at the Hawaii Ocean Time-series site. *Marine Chemistry* 60(1–2):33–47.

Wu LX, Cai WJ, Zhang LP, Nakamura H, Timmermann A, Joyce T, McPhaden MJ, Alexander M, Qiu B, Visbeck M, Chang P, Giese B. 2012. Enhanced warming over the global subtropical western boundary current. *Nature Climate Change* 2(3):161–6.

Yasuda I, Okuda K, Shimizu Y. 1996. Distribution and modification of North Pacific Intermediate Water in the Kuroshio-Oyashio interfrontal zone. *Journal of Physical Oceanography* 26(4):448–65.

Yasuda I. 2004. North Pacific Intermediate Water: Progress in SAGE (SubArctic Gyre Experiment) and Related Projects. *Journal of Oceanography* 60(2):385–95.

Yasunaka S, Nojiri Y, Nakaoka SI, Ono T, Mukai H, Usui N. 2014. North Pacific dissolved inorganic carbon variations related to the Pacific decadal Oscillation. *Geophysical Research Letters* 41(3):1005–11.